Schemes for the sound transmission of flat, curved and axisymmetric structures excited by aerodynamic and acoustic sources

F Errico, Mohamed Ichchou, F Franco, S de Rosa, Olivier Bareille, C Droz

Schemes for the sound transmission of flat, curved and axisymmetric structures excited by aerodynamic and acoustic sources

F. Errico[a,b,*], M. Ichchou[a], F. Franco[b], S. De Rosa[b], O. Bareille[a], and C. Droz[a]

[a] *Vibroacoustics & Complex Media Research Group, LTDS-CNRS UMR 5513, Ecole Centrale de Lyon, Écully, 69134, France*
[b] *Pasta-Lab, Dipartimento di Ingegneria Industriale, Universitá degli Studi di Napoli Federico II, Napoli, 80125, Italy*

Abstract

The paper describes a methodology for computing the sound transmission loss of any flat, curved and cylindrical, homogeneous and periodic structure, under any type of acoustic and/or aerodynamic load. An approximate excitation model is introduced to reproduce uncorrelated and spatially-correlated loads using a wavenumber integration of surface waves. Then, a wave finite element formulation is developed and interfaced with the excitation models in order to cover industrially-relevant case studies. Analytical, numerical and experimental transmission losses are presented for validation purposes. Finite size effects are also taken into account using a spatial windowing and a cylindrical analogy, for curved structures. Different periodic-cell designs are also compared and investigated under turbulent boundary layer and diffuse acoustic field excitations.

Keywords: Sound Transmission, Turbulent Boundary Layer, Periodic Structures, Curved Structures, Multi-Layered Structures

1. Introduction

Sandwich composite structures are extensively used in modern aerospace industry as well as in the automotive, naval and civil ones because they are lighter and stronger than most advanced panels in aluminium alloys. The anisotropy of such structures can be easily modified by changing the material and the shape of the core, obtaining different wave propagation properties. However, these types of structures are also known for having poor vibroacoustic performances which, often, can result in higher interior noise levels. This problem has a strong impact in many engineering areas, from space launchers to aircraft fuselages. Strong efforts have been recently placed on advanced methodologies for the the modelling of acoustic radiation of laminates and sandwich panels, since, classical models, using for example the finite element method (FEM), lead to cumbersome computational cost. Some FEM applications for the vibroacoustic analysis of simple structures, under random aeroacoustic loads, are present in literature [1, 2, 3, 4, 5].

An efficient alternative in terms of computational cost is, for example, the transfer matrix method (TMM). It is a general method used for the prediction of the propagation of monochromatic

*Corresponding author
Email address: fabrizio.errico@ec-lyon.fr (F. Errico)

plane waves in planar and multi-layered structures of infinite extent [6]. Many applications of the TMM to the modelling of sound trasmission of composite structures have already been validated [7, 8].

Finite size effects, important at low frequencies, can be included through appropriate corrections, leading to a broadband accuracy of the method [9, 10, 11].

Alternatively, the wave finite element method (WFE), specifically for homogeneous and periodic structures, allows the modelling of just a single repetitive cell, applying on it the periodicity conditions for a correct description of the entire (infinite) waveguide [12, 13, 14, 15, 16, 17]. The use of finite elements, for the cell description, enhances this method allowing the description of any type of complex structural shape, even in case of curvature [18, 19, 20, 21]. While mainly used for the analysis of the elastic waves' propagation in periodic media, the application of the WFEM for the sound transmission of sandwich panels has been recently proposed, under a plane wave load [22, 23] or diffuse acoustic load [24, 25], even though, to authors' knowledge, no application is available for curved and complex configurations, under general loads.

Within the frameworks of curved structures, alternative methods have also been presented. A mathematical model, for the transmission of airborne noise through the walls of an orthotropic cylindrical shell, has been firstly proposed by Koval, [26, 27, 28]. For curved composite laminates, the vibroacoustic problem has been further developed through a spectral approach based on a discrete lamina description, [29, 30]. Other semi-analytic approaches, based on a receptance method, have also been proposed in order to analyse the sound transmission of aircraft panels with stringers and ring frames, [31, 32].

Periodic structures and innovative material configurations (often indicated as meta-materials), on the other hand, can be used as frequency-selecting structures. The related waveguides, because of their complex shapes, require a higher computational cost for an accurate numerical simulation. In addition, the knowledge and the modelling of the correct operating conditions are fundamental in automotive and aerospace applications. For example, whenever a convective flow is present, boundary layer models should be included for completeness. None of the models in literature, at this stage, allows the analysis of complex structural periodic shapes, in presence of curvature and under aeroacoustic excitations, at the same time. For example, in the work of Yang et al. [23] only infinite flat homogenised structures can be analysed under plane waves' excitation. On the other hand, in the case of curved structures, the work of Kingan et al. [33] is limited to a single plane wave excitation, once a circumferential number is fixed; thus the sound transmission of complex curved structures under stochastic excitation can not be obtained, in this case.

The novelty of the present paper stands in overcoming some of these limits proposing a methodology for dealing with a wider range of case-studies, under operational conditions: space launcher fairings, fuselage panels, pipes, ducts and acoustic barriers. Periodic flat, curved and cylindrical structural designs can be compared in terms of their vibroacoustic performance, under any desired convective and acoustic load.

The paper is structured as follows: Section 2 presents a theoretical background of the WFE

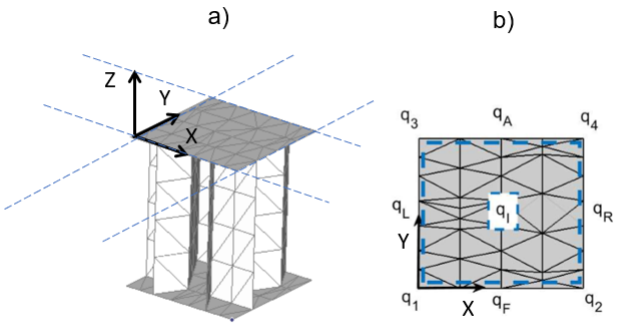

Figure 1: Example of a FE cell model with periodicity along the X-Y directions. a) Isometric view; b) Top view with nodes' subsets.

method; Section 3 describes the proposed load approximation and the wavenumber integration, to take into account a general fluid excitation; Sections 4 and 5 are devoted to the validations for both the acoustic and aerodynamic load; Section 6 presents an analysis of the proposed approximations and a discussion the advantages and limits of the approach. It is finally shown a comparison for the effective transmission loss of periodic cylinders as enabled by the presented method.

2. The Wave Finite element Method

A 2D periodic structure is composed by an assembly, along arbitrary directions, of identical elementary cells. Using any FE commercial code, the mass and stiffness matrices of the cell, whenever complex, can be extracted and post-processed. Of course, since being FEs, all classic meshing considerations for an appropriate wavelength description are valid. With reference to Fig. 1, the dynamic stiffness equation of the segment can be written as

$$[\mathbf{K} - \omega^2 \mathbf{M}]\mathbf{q} = \mathbf{D}\mathbf{q} = \mathbf{f} + \mathbf{e} \tag{1}$$

where $\mathbf{q}$, $\mathbf{f}$ and $\mathbf{e}$ are respectively the nodal vectors of degrees of freedom (DoFs), internal and external forces; $\mathbf{K}$, $\mathbf{M}$ and $\mathbf{D}$ are the stiffness, mass and dynamic stiffness matrices. Damping can be modelled by including, in Eq. (1), appropriate complex matrices and/or coefficients. In this paper, it is assumed that the vectors and matrices are ordered following the same sequence of the DoFs nodal vector: $\mathbf{q} = [\mathbf{q}_I, \mathbf{q}_F, \mathbf{q}_L, \mathbf{q}_1, \mathbf{q}_A, \mathbf{q}_R, \mathbf{q}_2, \mathbf{q}_3, \mathbf{q}_4]$. The wave motion through a periodic media can be analysed by imposing the Bloch-Floquet conditions [12, 13] to the finite element (FE) of a periodic cell, assuming time and space harmonic excitation. The periodicity conditions are translated in a magnitude and phase link among each point belonging to the periodic pattern, using a complex propagating constant for each wave type.

Displacements and forces at any point of the cell can be connected to the ones of a limited

number of them, as follows:

$$\begin{bmatrix} \mathbf{q}_A \\ \mathbf{q}_R \\ \mathbf{q}_2 \\ \mathbf{q}_3 \\ \mathbf{q}_4 \end{bmatrix} = \begin{bmatrix} \mathbf{0} & \mathbf{I}\lambda_Y & \mathbf{0} & \mathbf{0} \\ \mathbf{0} & \mathbf{0} & \mathbf{I}\lambda_X & \mathbf{0} \\ \mathbf{0} & \mathbf{0} & \mathbf{0} & \mathbf{I}\lambda_X \\ \mathbf{0} & \mathbf{0} & \mathbf{0} & \mathbf{I}\lambda_Y \\ \mathbf{0} & \mathbf{0} & \mathbf{0} & \mathbf{I}\lambda_X\lambda_Y \end{bmatrix} \begin{bmatrix} \mathbf{q}_I \\ \mathbf{q}_F \\ \mathbf{q}_L \\ \mathbf{q}_1 \end{bmatrix} \tag{2}$$

with

$$\lambda_X = \mathrm{e}^{-\mathrm{i}k_X L_X} \qquad \lambda_Y = \mathrm{e}^{-\mathrm{i}k_Y L_Y} \tag{3}$$

where k_X and k_Y are wavenumbers of the propagating (or forcing) wave in the periodicity directions X and Y, while L_X and L_Y represent the cell lengths along the same directions. The matrix $\mathbf{I}$ is, instead, the identity matrix. In a general form, thus, the total displacements and forces are connected to the reduced vectors (superscript red) through a periodicity matrix $\mathbf{\Lambda}$ (see Eq. (2)):

$$\mathbf{q} = \mathbf{\Lambda}\mathbf{q}^{\mathrm{red}} \qquad \mathbf{f} = -\mathbf{\Lambda}\mathbf{f}^{\mathrm{red}} \qquad \mathbf{e} = -\mathbf{\Lambda}\mathbf{e}^{\mathrm{red}} \tag{4}$$

Pre-multiplying Eq. (1) by $\mathbf{\Lambda}^{\mathrm{H}}$, where H stands for the hermitian operator, the dynamic stiffness matrix of the reduced model is given by Eq. (5):

$$\mathbf{D}_S = \mathbf{\Lambda}^{\mathrm{H}}[\mathbf{K} - \omega^2\mathbf{M}]\mathbf{\Lambda}. \tag{5}$$

The linearity of the stress tensor with respect to the displacement field, in addition to the periodicity relations, leads to an equilibrium of the internal forces between neighbouring cells; thus only external forces are considered.

At this stage, different eigenvalue problems can be solved, if the target is the estimation of the dispersion curves of the periodic structure, [14, 34].

2.1. Modal Order Reduction: A Craig-Bampton Scheme

The use of modal reduction is highly suggested for very fine meshes. In these cases, the internal degrees of freedom, defined before as $\mathbf{q}_I$, are substituted by the modal participation factors [35, 36]. Here an example of component mode synthesis (CMS) procedure, performed at the cell's scale, is shown. The aim of the CMS procedure is to achieve a significant reduction of the number of inner DOFs, by replacing displacements with the local modes of the cell. Here, the displacement vector $\mathbf{q}$ defined in Eq. (1), is partitioned into the inner displacements, $\mathbf{q}_{In}$, and boundary displacements, $\mathbf{q}_B$. In this specific case, since the nodes belonging to the top and bottom of the cell are used for load translation, as shown in subsection 2.3, $\mathbf{q}_{In}$ is a subset of the $\mathbf{q}_I$ in Eq. (2). By using this division, Eq. (1) takes the form of Eq. (6):

$$\left(\begin{bmatrix} \mathbf{K}_{BB} & \mathbf{K}_{BIn} \\ \mathbf{K}_{InB} & \mathbf{K}_{InIn} \end{bmatrix} - \omega^2 \begin{bmatrix} \mathbf{M}_{BB} & \mathbf{M}_{BIn} \\ \mathbf{M}_{InB} & \mathbf{M}_{InIn} \end{bmatrix} \right) \begin{bmatrix} \mathbf{q}_B \\ \mathbf{q}_{In} \end{bmatrix} = \begin{bmatrix} \mathbf{f}_B \\ \mathbf{0} \end{bmatrix}, \tag{6}$$

where $\mathbf{f}_{In}$ is zero, since no load is applied on this subset of nodes. The reduced basis involves the static boundary modes $\mathbf{\Psi}_B$ and component modes $\mathbf{\Psi}_C$.

In this way the final displacements vector can be re-written as:

$$\begin{bmatrix} \mathbf{q}_B \\ \mathbf{q}_{In} \end{bmatrix} = \mathbf{G} \begin{bmatrix} \mathbf{q}_B \\ \mathbf{P}_{In} \end{bmatrix}; \qquad \mathbf{G} = \begin{bmatrix} \mathbf{I} & \mathbf{0} \\ \mathbf{\Psi}_B & \mathbf{\Psi}_C \end{bmatrix} \tag{7}$$

where $\mathbf{I}$ and $\mathbf{0}$ are the identity and zero matrix respectively, and $\mathbf{P}_{In}$ is the set of retained modal participation factors. The static boundary modes $\mathbf{\Psi}_B$ and component modes $\mathbf{\Psi}_C$ can be derived from Eq. (8),

$$\mathbf{\Psi}_B = \mathbf{K}_{InIn}^{-1}\mathbf{K}_{InB}; \qquad (\mathbf{K}_{InIn} - \omega^2\mathbf{M}_{InIn})\mathbf{\Psi}_C = \mathbf{0}. \tag{8}$$

In the Craig-Bampton (CB) approach, the modal selection is based on the lower resonance frequencies. This method has been extended in a wave approach context, when the aim is to capture the local deformed shape of the periodic unit cell. This means that the displacements inside a unit-cell can be expanded on a subset of stationary modes [35, 36].

Finally the stiffness and mass matrices, that can be post-processed a-priori if curvature has to be simulated (see subsection 2.2), can be written in the reduced set of coordinates using the projection matrix $\mathbf{G}$ defined by Eq. (7):

$$\begin{aligned} \mathbf{M}_{\text{Cond}} &= \mathbf{G}^{\text{T}}\mathbf{M}\mathbf{G} \\ \mathbf{K}_{\text{Cond}} &= \mathbf{G}^{\text{T}}\mathbf{K}\mathbf{G}. \end{aligned} \tag{9}$$

The set of retained modal participation factors, $\mathbf{P}_{In}$, can be, then, statically condensed at each frequency step.

2.2. Curvature Simulation

Curved structures deserve also some interest. Here a method, to take into account the curvature effects, is presented. With reference to Fig. 2, the idea is to rotate the local reference for each node belonging to the cell FE. This way, imposing the periodicity conditions, as shown in Eq. (3) and (4), the wave propagation is automatically analysed along the imposed curved path. Each translational DoF is rotated depending on its distance from the axis of rotation. A single FE model of the cell can be used to simulate different curvatures, and, apart from large periods, the cell can be modelled as totally flat.

In order to achieve the model of the curved cell, a rotational matrix $\mathbf{r}$ is defined and assembled in a block diagonal matrix, $\mathbf{Rot}$. It is intended to be done for each curvature and the effects can be superimposed [37]; in the present analysis, a single curvature is considered. Hence, the mass and stiffness matrices of the curved waveguide are obtained as:

$$\begin{aligned} \mathbf{M}_{\text{curv}} &= \mathbf{Rot}^{\text{T}}\mathbf{M}_{\text{flat}}\mathbf{Rot} \\ \mathbf{K}_{\text{curv}} &= \mathbf{Rot}^{\text{T}}\mathbf{K}_{\text{flat}}\mathbf{Rot}, \end{aligned} \tag{10}$$

where $\mathbf{Rot}$ is the rotation matrix, while the subscript $flat$ refers to the FE matrices of the periodic cell being modelled as flat and the subscript *curv* to the ones calculated simulating the curvature of the system. The waves analysed along the locally curved reference (X' in Figs. 2 and 3) are circumferential waves. Forcing wavenumbers, imposed after Eq. (10), represent, in general, helical

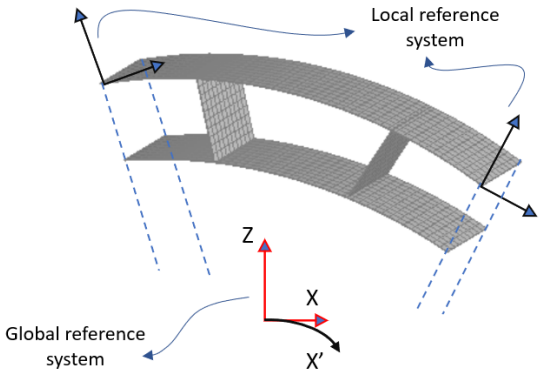

Figure 2: Rotation of the local system of reference for each node of the periodic cell FE model

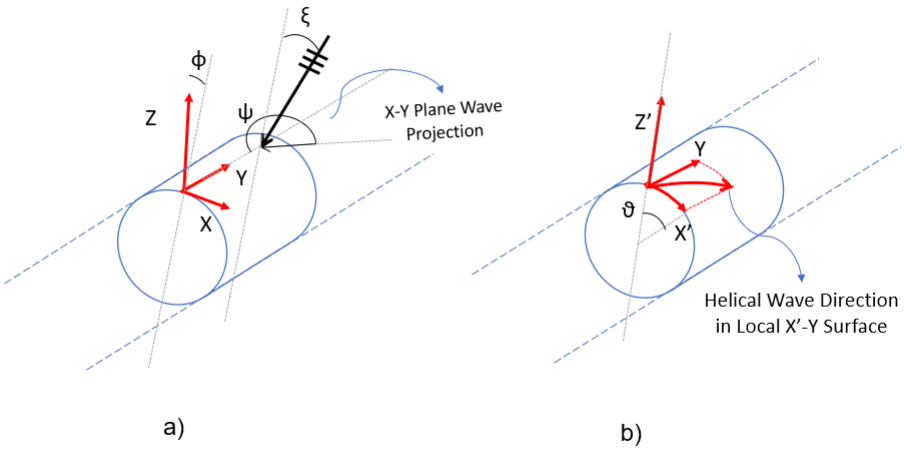

Figure 3: Global and Local reference systems used for waves along curved structures and shells. a) Global Cartesian reference; b) Local Curved Reference.

waves exciting the semi-infinite cylindrical panel/shell (Fig. 3). It is worth to emphasize that the curvature simulation, showed here, aims at connecting the edge sections of the unit cell through a curved (discrete) system of coordinates. If point of inflections are present, at cell scale, depending on the structure to be described, two approaches are possible, once the cell is modelled with the inflected parts. In one case, the wave propagation can be analysed along the global X-Y axes, simulating a flat waveguide with inflected sections. Otherwise, the cell curvature can be simulated using the nodal coordinates, even the ones belonging to the inflected part of the cell, to evaluate the local rotation of the coordinate system to be simulated; this is translated in a rotation matrix in Eq. (10).

2.3. Fluid-Structure Coupling

Let us assume a forcing wave impinging on one face of the structure, with an amplitude p_I. The structure, as a result, transmits and reflects waves in the fluid adjacent to the top and bottom surfaces. On the excited side (subscript 1), the sound field is the superposition of the incident and reflected acoustic sound waves, while, in the receiver side (subscript 2), it is given by the transmitted waves.

Assuming the X-Y as the plane of reference (Fig. 1 as example), a forcing acoustic pressure wave can be defined, on the surface of the cell, omitting the time harmonic dependence for simplicity, as (see Fig. 3a):

$$\begin{aligned} \text{Flat Surface} : PW &= p_I \mathrm{e}^{-\mathrm{i}(k_X X + k_Y Y - k_{Z,1} Z)}; \\ \text{Curved Surface} : HW &= p_I \mathrm{e}^{-\mathrm{i}(k_X R \sin\Phi + k_Y Y - k_{Z,1} R \cos\Phi)}; \end{aligned} \tag{11}$$

where, k_X, k_Y and k_Z are the projections in the global X-Y-Z reference of the plane wave (see Fig. 3a). Here, in the case of curved surfaces, as described also in subsection 2.2, the assumed plane wave is approximated through its projection components on the locally curved surface (Fig. 3b):

$$HW = p_I \mathrm{e}^{-\mathrm{i}(k_{X'} X' + k_Y Y - k_{Z',1} Z')} \approx p_I \mathrm{e}^{-\mathrm{i}(k_\theta \theta + k_Y Y - k_R Z')}; \tag{12}$$

where $k_{X'}$ k_Y and $k_{Z'}$ are the wavenumber components in the new locally rotated reference (see Fig. 3b) and are directly proportional to the circumferential, axial and radial wavenumber components, respectively. It is worth to emphasize that a typical decomposition in cylindrical waves, implying the use of Bessel functions, is not necessary when using a locally rotated reference system as the one in Fig. 3b: Eq. (12) depicts helical waves in cylindrical coordinates and the equivalent plane waves in cartesian coordinates, respectively [14, 19, 20, 21].

From now on, the approximated representation of Eq. (12) is used independently on the curvature of the structural model; for infinite radius of curvature (flat structure), the local and global reference system coincide.

If in-plane homogeneous layers are assumed, the local wavenumber components k_X and k_Y are conserved along the structure, and the only parameter which can vary with the nature of the fluid (or the excitation) is the k'_Z component, derivable using the Helmholtz equation. When

non-homogenised periodic cells are considered, multiple harmonics are added to the k_X and k_Y terms [38]. In this framework, the multiple harmonics that arise for periodic non-homogenised structures, are numerically accounted in the structural response of the radiating side (subscript 2). In fact, when applying the WFE, discrete periodic conditions are applied for the forcing (see Eq. (11)) wavenumber couples k_X and k_Y (see Eqs. (2), (3) and (4)) and for each node subset; the resulting free or forced structural vibration includes any periodicity effects in the frequency band of analysis.

To express the nodal forces on the periodic cell as a function of the pressure amplitudes in the forcing and radiating side of the structure, the dynamic stiffness of the fluids must be derived. From continuity of the normal particle velocity on the excited and radiating surfaces:

$$\begin{aligned} \rho_1\omega^2 q_{\text{in}} &= \frac{\partial(p_I - p_R)}{\partial z}; \qquad D_{f,1} = \frac{-\mathrm{i}\rho_1\omega^2}{k_{Z,1}} \\ \rho_2\omega^2 q_{\text{rad}} &= \frac{\partial(p_T)}{\partial z}; \qquad D_{f,2} = \frac{-\mathrm{i}\rho_2\omega^2}{k_{Z,2}} \end{aligned} \tag{13}$$

where ρ_1 and ρ_2 are the fluid densities, q_{in} and q_{rad} are the out-of-plane displacements, respectively of the incident and radiating surfaces, and $D_{f,1}$ and $D_{f,2}$ the dynamic stiffness of the fluid in the incident and radiating domains; p_I, p_R and p_T are the incident, reflected and transmitted amplitudes of the sound pressure waves. It is important to notice that, regardless of the homogeneity of the structural model, the derivations over Z, in Eq. (13), makes the modelling of the radiating acoustic field somewhat non-sensitive to the presence or absence of multiple harmonics which might arise due to heterogeneity of the structure. These effects are included in the dynamic stiffness of the cell in Eq. (5) and are accounted in the structural response.

The load imposed on the plate, by the forcing surface waves of trace wavenumbers k_X and k_Y, can be derived from the two pressure fields, on both sides of the structure; it is lumped on the wetted nodes of the finite element model. As the forces act normal to the surfaces, the only excited degrees of freedom are the ones connected to the out-of-plane displacements. These ones are identified with the subscript T (top) and B (bottom), while all other degrees of freedom (not excited) are identified by I (internal). The vector of the external forces can be written as:

$$\begin{bmatrix} \mathbf{e}_T^{\text{red}} \\ \mathbf{e}_I^{\text{red}} \\ \mathbf{e}_B^{\text{red}} \end{bmatrix} = \begin{bmatrix} \mathbf{S}\cdot(\mathbf{p}_I + \mathbf{p}_R) \\ \mathbf{0} \\ \mathbf{S}\cdot\mathbf{p}_T \end{bmatrix} \tag{14}$$

where $\mathbf{S}$ is vector of the free nodal surface of each excited node and $\mathbf{p}_I$, $\mathbf{p}_R$ and $\mathbf{p}_T$ are the nodal pressure vectors. A finer way to calculate consistent nodal forces, requires, however, the knowledge of the shape functions associated with the out-of-plane displacements [23]. The dynamic stiffness matrix and the reduced displacement vector can be rearranged in the same way as in Eq. (14), then an energetic equivalence through-thickness applied, condensing all the non-excited nodes [8]. Including the relation of Eq. (13), the dynamic problem results in:

$$\begin{bmatrix} \mathbf{D}^c_{S_{TT}} & \mathbf{D}^c_{S_{TB}} \\ \mathbf{D}^c_{S_{BT}} & \mathbf{D}^c_{S_{BB}} \end{bmatrix} \begin{bmatrix} \mathbf{p}_I - \mathbf{p}_R \\ \mathbf{p}_T \end{bmatrix} = \begin{bmatrix} \mathbf{S}\cdot\mathbf{D}_{f,1}\cdot(\mathbf{p}_I + \mathbf{p}_R) \\ \mathbf{S}\cdot\mathbf{D}_{f,2}\cdot(\mathbf{p}_T) \end{bmatrix} \tag{15}$$

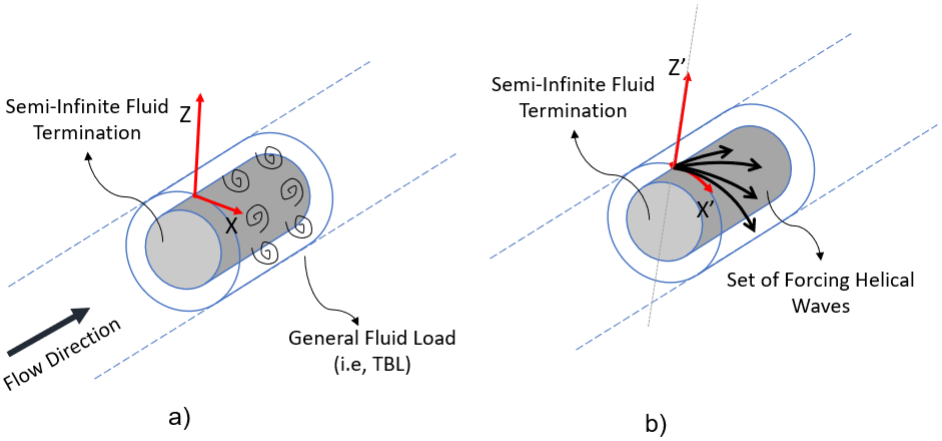

Figure 4: Illustration of the load simulation using surface waves in a general test-case. a) Real/Physical situation; b) Simulated case.

where the superscript c indicates that the original $\mathbf{D}_S$ matrix (Eq. (5)) is condensed for the non excited (I) degrees of freedom, through the thickness. The algebraic system in Eq. (15) can be solved in $\mathbf{p}_R$ and $\mathbf{p}_T$ obtaining the power transmission coefficient τ associated with the couple of forcing wavenumbers k_X and k_Y.

$$\tau(k_X, k_Y) = \frac{(k_{Z,2}/\rho_2)\mathbf{S}|\mathbf{p}_T^2|}{(k_{Z,1}/\rho_1)\mathbf{S}|\mathbf{p}_I^2|}. \tag{16}$$

Finite size effects, can be included through correction factors, in order to increase the accuracy at low frequencies. While a formal and accurate spatial windowing approach is present in literature [9], the computational cost associated with this step might be high. For this reason, even losing some accuracy in the low frequency bandwidth range, the use of asymptotic formulas, as in [10], is here used to reduce the computational cost.

3. Stochastic Load Translation into Surface Waves

The sound transmission to plane wave excitation, as discussed in Sec. 2, is not sufficient for many applications. Herein, a method, to take into account a general type of excitation, is proposed. An illustration is reported in Fig. 4. The idea is to use a forcing surface wave excitation for each couple of forcing wavenumbers k_X and k_Y, able to represent the desired excitation, once its wall pressure spectra, in the wavenumber domain, is known. Using a vectorial form and omitting the harmonic dependence for the sake of readability, a sum of wall plane waves can be written as:

$$P(\bar{X}) = \sum_{j=1}^{N_W} A_j \mathrm{e}^{-\mathrm{i}\bar{K}_j\bar{X}}. \tag{17}$$

where $\bar{X}$ stands for the couple of surface coordinates (i.e. X–Y in Fig. 1), $\bar{K}_j$ is the wavenumber vector associated with each wall surface wave of amplitude A_j, and N_W is the total number of waves constituting the pressure field. It is worth recalling that the surface coordinates can be the global coordinates, if the structure is flat, or, equivalently, the local coordinates if a curvature is

present. In the first case, Eq. (17) is physically representative of the classic sum of plane waves. In the other case, it reports a sum of wall helical waves on the curved cylindrical structures.

The description of the desired load is based on the knowledge of the proper values of $\bar{K}_j$ and A_j (Eq. (17)). They are obtained by equating the wavenumber spectra ϕ_{PP}, of the pressure field (Eq. (17)), with the one of the fluid excitation model to be simulated, Φ_{PP}, for a specific fluid wavenumber $\bar{K}$. Many fluid excitation models are investigated in the wavenumber domain in literature [39]. The cross correlation of the pressure field P is:

$$R_{PP}(\Delta\bar{X}_1, \Delta\bar{X}_2) = \sum_{j=1}^{N_W} A_j^2 \mathrm{e}^{-\mathrm{i}\bar{K}_j(\Delta\bar{X}_1 - \Delta\bar{X}_2)} + \sum_{j=1}^{N_W} \sum_{n=1;n\neq j}^{N_W} A_j A_n \mathrm{e}^{-\mathrm{i}(\bar{K}_j\Delta\bar{X}_1 - \bar{K}_n\Delta\bar{X}_2)} \tag{18}$$

where the auto and cross correlations have been divided in two different summations. Performing the Fourier transform of Eq. (18), the wavenumber spectra is obtained:

$$\begin{aligned} \phi_{PP}(\bar{K},\omega) = \Phi_{PP}(\bar{K},\omega) = \frac{1}{4\pi^2}\Bigg(\sum_{j=1}^{N_W} A_j^2 \left[\frac{\mathrm{e}^{\mathrm{i}(\bar{K}_j - \bar{K})(\Delta\bar{X}_1 - \Delta\bar{X}_2)}}{\mathrm{i}(\bar{K}_j - \bar{K})}\right]_{-\infty}^{+\infty} \\ + \sum_{j=1}^{N_W} \sum_{n=1;n\neq j}^{N_W} A_j A_n \left[\frac{\mathrm{e}^{\mathrm{i}(\bar{K}_j - \bar{K})(\Delta\bar{X}_1)}}{-\mathrm{i}(\bar{K}_j - \bar{K})}\right]_{-\infty}^{+\infty} \left[\frac{\mathrm{e}^{\mathrm{i}(\bar{K}_n - \bar{K})(\Delta\bar{X}_2)}}{-\mathrm{i}(\bar{K}_n - \bar{K})}\right]_{-\infty}^{+\infty}\Bigg). \end{aligned} \tag{19}$$

The expressions in Eq. (19) are known and can be written as Dirac *delta*-functions. Moving from summations and after some algebra, the final expression of ϕ_{PP} is given in Eq. (20). The second term in Eq. (20) can be erased since, by definition, the correlation indices j and n must be different while the integration of the product of the Dirac functions is not null only for $\bar{K}_j = \bar{K}_n$.

$$\begin{aligned} \phi_{PP}(\bar{K}) = \Phi_{PP}(\bar{K}) = \int 4\pi^2 \frac{A_j^2}{\Delta\bar{K}_j} \delta(\bar{K}_j - \bar{K}) \mathrm{d}\bar{K}_j \\ + \int\int 8\pi^4 \frac{A_j A_n}{\Delta\bar{K}_j \Delta\bar{K}_n} \delta(\bar{K}_j - \bar{K}) \delta(\bar{K}_n - \bar{K}) \mathrm{d}\bar{K}_j \mathrm{d}\bar{K}_n \end{aligned} \tag{20}$$

The amplitudes and the wavenumbers of the simulated waves, able to describe a fluid excitation with the wavenumber spectra Φ_{PP}, are straightforwardly obtainable from Eq. (20). For each forcing k_X and k_Y, the desired loading model is simulated through the following surface wave:

$$P_W(X, Y, \omega) = \sqrt{\frac{\Phi_{PP}(k_X, k_Y, \omega)\Delta k_X \Delta k_Y}{4\pi^2}} \mathrm{e}^{-\mathrm{i}(k_X X + k_Y Y)}. \tag{21}$$

In conclusion, at each frequency and for each wavenumber of the fluid excitation model, a surface wave of specific wavenumbers and amplitudes can be used to simulate the load. No hypothesis on the correlation of the forcing waves is imposed as for the reference coordinates. The proposed approximation is thus valid for correlated and uncorrelated loads acting on plane and curved surfaces, independently on their complexity.

3.1. Sound Transmission Loss

In order to simulate the sound transmission for a specific excitation, an integration of the transmission coefficient is performed, in the wavenumber domain. Thus, the total transmission coefficient can be calculated as follows:

$$\tau_{TOT}(\omega) = \frac{\int\int \tau(k_X, k_Y) \times W_A(k_X, k_Y, \omega) \mathrm{d}k_X \mathrm{d}k_Y}{\int\int W_A(k_X, k_Y, \omega) \mathrm{d}k_X \mathrm{d}k_Y} \tag{22}$$

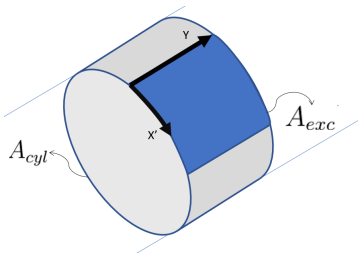

Figure 5: Excited surface comparison between a curved finite panel and its equivalent cylindrical portion.

where W_A is the element corresponding to the wall surface wave of wavenumbers k_X and k_Y, in the matrix of the normalized amplitude functions of all the wavenumber couples involved in the integration process. Within the framework of sound transmission, as identifiable from Eq. (16), the variation of waves amplitudes does not have an influence. The difference among different fluid loads is given by the weighting functions W_A being involved in the integration. The convergence of the method is assured by the convergence of the integration process. The choice of the integration limits can be changed depending on the type of load to be described. For example, for a diffuse acoustic field, at each frequency step, the wavenumber spectra Φ_{PP} is null outside the acoustic border, so, there is no need for the use of higher integration limits. The final transmission loss is, by definition:

$$\mathrm{TL}(\omega) = -10\log_{10}(\tau_{\mathrm{TOT}}(\omega)) \tag{23}$$

The TL expression in Eq. (23) includes the assumption, if a curvature is simulated, that the excited surface is a plan projection of the shell surface. The transmission coefficient in Eq. (22), must be multiplied by the ratio of cylindrical section and its plan projection. However, in the case of curved finite structures, instead of using a baffled window equivalence, for accounting the effects of the finiteness of the structure, an alternative approach based on the ratio of the excited surfaces is here proposed. With reference to Fig. 5, the ratio between the area of the equivalent cylindrical portion (A_{cyl}), built starting from the finite curved panel analysed, and the effectively excited area (A_{exc}), is multiplied, in a SEA (Statistical Energy Analysis) fashion, to the transmission coefficient in Eq. (22). The approach is consistent since, given a certain length of the panel, along the non-curved side, its area can increase just up to the one of the equivalent cylindrical portion. The resulting TL, thus, can asymptotically converge toward the one of the equivalent cylinder. In these cases, Eq. (23) becomes:

$$\mathrm{TL}(\omega) = -10\log_{10}\left(\tau_{\mathrm{TOT}}(\omega)\frac{\pi A_{\mathrm{cyl}}}{2A_{\mathrm{exc}}}\right). \tag{24}$$

The advantage of the present approach relies in its generality and applicability to a wide range of test-cases both in terms of structural shapes and excitation models. The wall surface wave approximation releases the constraints to the plane waves angles of incidence, generally implied in literature, widening the analysable combinations of structural and excitation models. On the structural point of view, the only requirement, for the applicability of the present approach, is given by the homogeneity or periodicity, independently on the reference direction (flat or curved). On the other hand, for the simulated excitation, the basic requirement is the knowledge of the wall

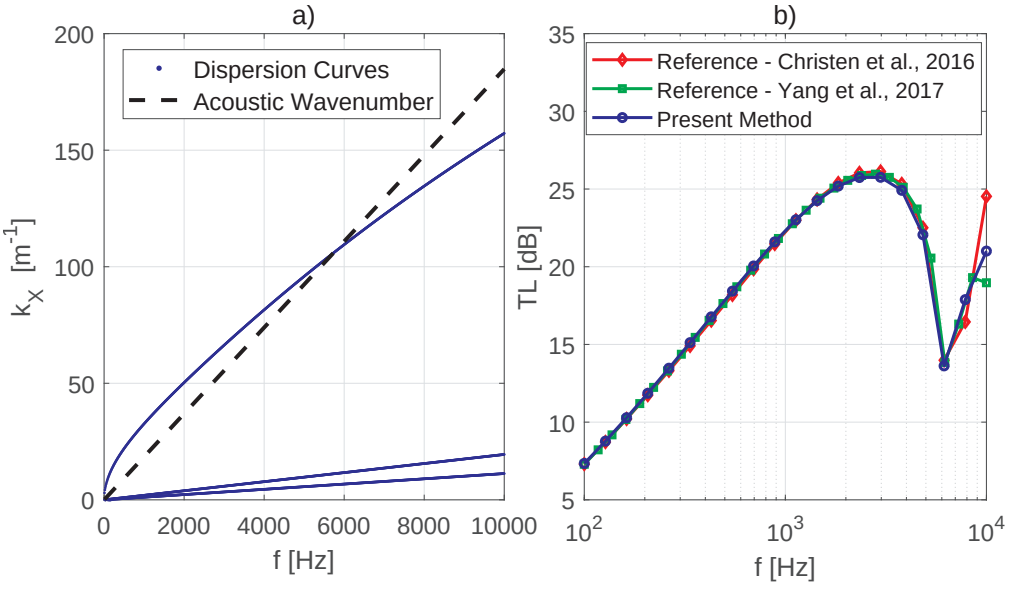

Figure 6: A sandwich flat panel under diffuse acoustic field excitation. a) Dispersion curves; b) Transmission Loss comparison with literature references ([22, 23]) in a logarithmic frequency step, between 100 Hz and 10KHz.

pressure spectrum.

4. Validation for Diffuse Field Transmission

In this section, a series of comparisons are presented for validation purposes. Both flat and curved composite sandwich panels are analysed. A validation for cylinders is also present, under diffuse acoustic loading. In all the test-cases proposed here, the dispersion curves in the in the X and Y direction (Fig. 1,2) will be provided in order to observe acoustic coincidences in terms of waves.

4.1. Flat Homogenised Panel

In Fig. 6, a comparison among the proposed method and two other approaches available in literature is shown [22, 23]. The analysed sample is a 3mm thick flat sandwich panel made of 1mm-thick aluminium skins and a 1.5mm-thick isotropic core ($E = 3$ GPa, $\nu = 0.2$, $\rho = 48$ Kg/m^3). The cell is modelled using four ANSYS solid elements through thickness. The dispersion curves in Fig. 6a, show an acoustic coincidence at ≈ 6 kHz. In Fig. 6b an excellent agreement is observed for the sound transmission loss calculated using the present approach and the numerical ones in [22, 23]. Finite size effects are not included in the model and thus the comparisons in Fig. 6 are for infinite panels.

4.2. Flat Heterogeneous Panels

The second test-cases consist in an aluminium double-wall flat panel with mechanical connections (Fig. 7a), and a sandwich panel with rectangular core (Fig. 7b) made in ABS ($E = 1.8$ GPa, $\nu = 0.35$, $\rho = 998$ Kg/m^3).

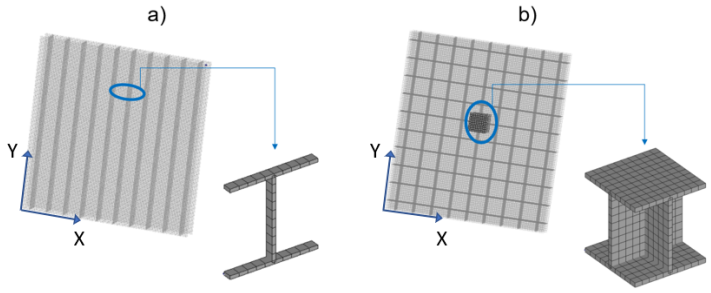

Figure 7: Portion of a double wall flat panel with structural links and the detail of the unit cell analysed

The dispersion curves of the two test-cases analysed are plotted in Fig. 8 with the acoustic wavenumbers versus frequency. The wavenumbers are derived from the propagations constants which are solutions of the eigenvalue problem in Eq. (5). Respectively, Fig. 9a shows the comparison for the TL, using an in-house reproduced code of the method presented by Christen et al. [22], whereas, Fig. 9b, shows the comparison for the TL of the sandwich rectangular-cored panel using, as a reference, the transfer matrix approach proposed by Parrinello et al. [8]. The double-wall cell is 5mm thick, 10mm long in the periodic direction (X), 1mm long in the homogeneous direction (Y) and the walls have a thickness of 1mm. The rectangular cored sandwich cell is 10mm thick, 10mm long both in X and Y, the skins and the core walls have a thickness of 0.6mm. Finite size effects are not included in the model and thus the comparisons in Fig. 6 are for infinite panels. Again excellent agreement is observed, even for this complex structural shape, validating the proposed approach also for large heterogeneity scales and non-homogenised structure models. In this case, ANSYS *shell* elements are used instead, for the FE modelling. In all presented results, the mesh used for the calculations is verified to converge in the frequency band investigated.

4.3. Curved Homogenised Panels and Cylinders

The presence of curvature induces an alteration in the structural behaviour, at least, up to the ring frequency. This is the eigenfrequency corresponding to the first extensional mode at which the longitudinal wavelength is equal to the circumference of the structural element. At this frequency, the shell sound radiation is amplified similarly to a coincidence condition [26]. The transmission of curved panels and cylinders is here validated, under diffuse acoustic load, using, as a reference, numerical and experimental data available in literature.

The shell is a 3mm thick aluminium one and the curvature radius is 2m and the dispersion curves versus the acoustic wavenumbers are reported in Fig. 10a. First, in Fig. 10b, the transmission loss of an infinite cylinder is compared to the numerical work by Ghinet [30]. Both the ring frequency ($\approx$ 400 Hz; see Fig. 10a) and the acoustic coincidence ($\approx$ 4.0 kHz; see Fig. 10a) are accurately described and the overall agreement is excellent.

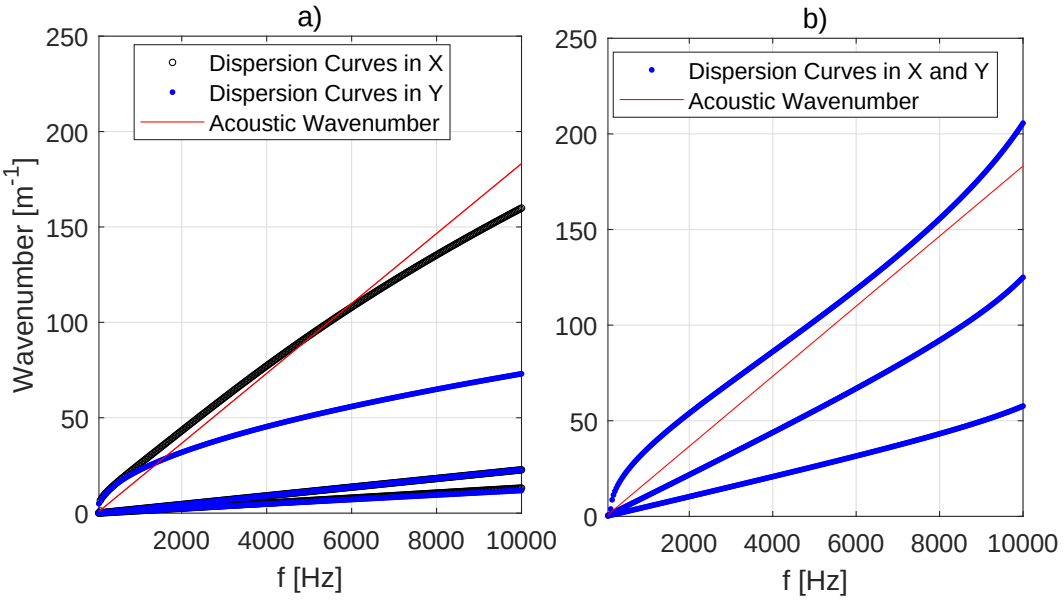

Figure 8: Dispersion Curves for the sandwich panel designs in Fig. 7. The wavenumbers represent derive from the eigenvalues of Eq. (5): a) Double-wall panel with structural link; b) Sandiwch panel with rectangular core.

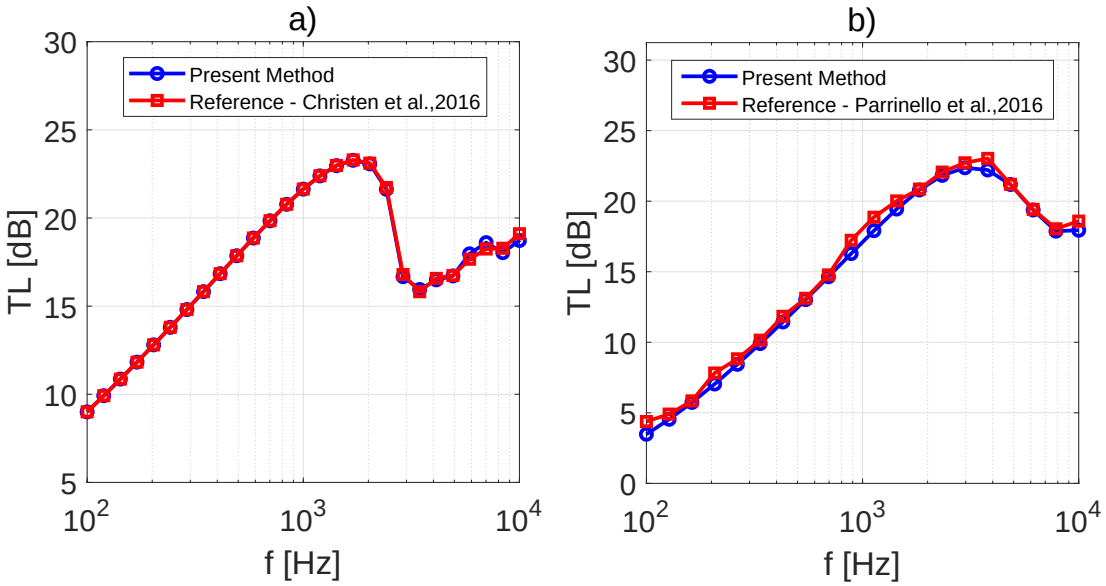

Figure 9: Transmission Loss comparison for the sandwich panel designs in Fig. 7, under diffuse acoustic field excitation. A logarithmic frequency step, between 100 Hz and 10KHz, is used to generate the curve labelled as *Present Method*. a) Reference method in [22]; b) Reference method in [8]

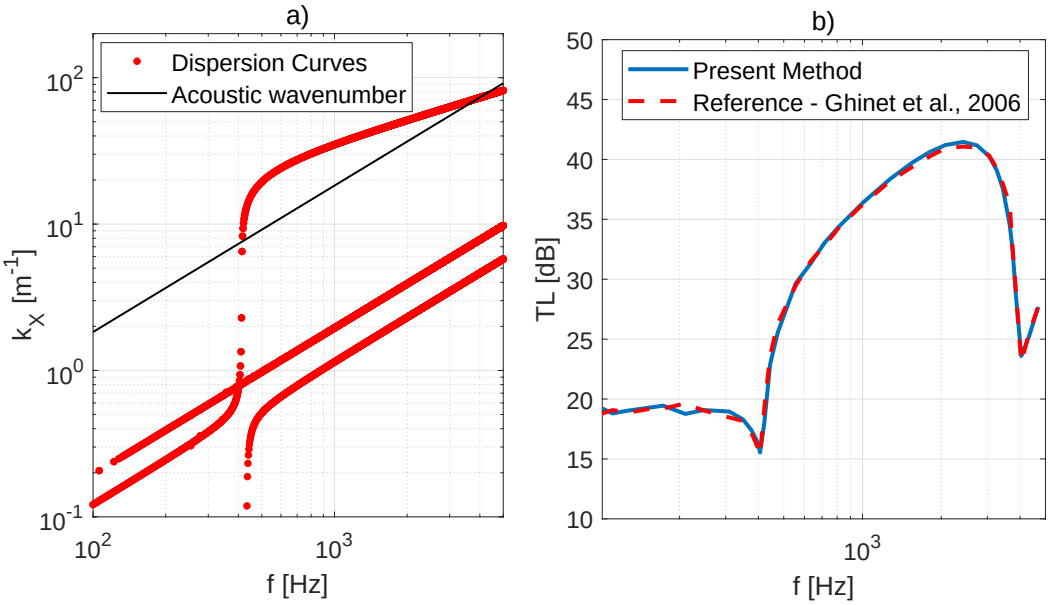

Figure 10: An isotropic cylinder under diffuse acoustic field excitation. a) Dispersion curves; b) Sound Transmission Loss comparison with numerical results form [30].

Table 1: Materials' properties for curved finite panels transmission loss validation

	Skin	Core
E_1 (GPa)	48.0	0.145
$G_{1,2}$ (GPa)	18.1	0.05
$G_{1,3}$ (GPa)	2.75	0.05
$\nu_{1,2}$	0.3	0.2
ρ (Kg/m^3)	1550.0	110.44

On the other hand, in Figs. 11, a validation versus experimental measurements for curved finite panels is shown. In both cases the curvature radius is 2m; the skin and core material are reported in Table 1.

Fig. 11b shows the sound transmission loss for a 2x2.4m^2 sandwich composite panel whose skin and core are, respectively, 1.2mm and 12.7mm thick. The present method leads to a very good agreement even in the low frequency range. Again, both the ring frequency ($\approx$ 400 Hz) and the acoustic coincidence ($\approx$ 1.0 kHz), observable from the dispersion curves in Fig. 11a, are well predicted.

The proposed validations demonstrate the accuracy for both the methodology to account for curvature effects and the proposed approach to include finite size effects in the case of curved structures (Eq. (24) is used here) .

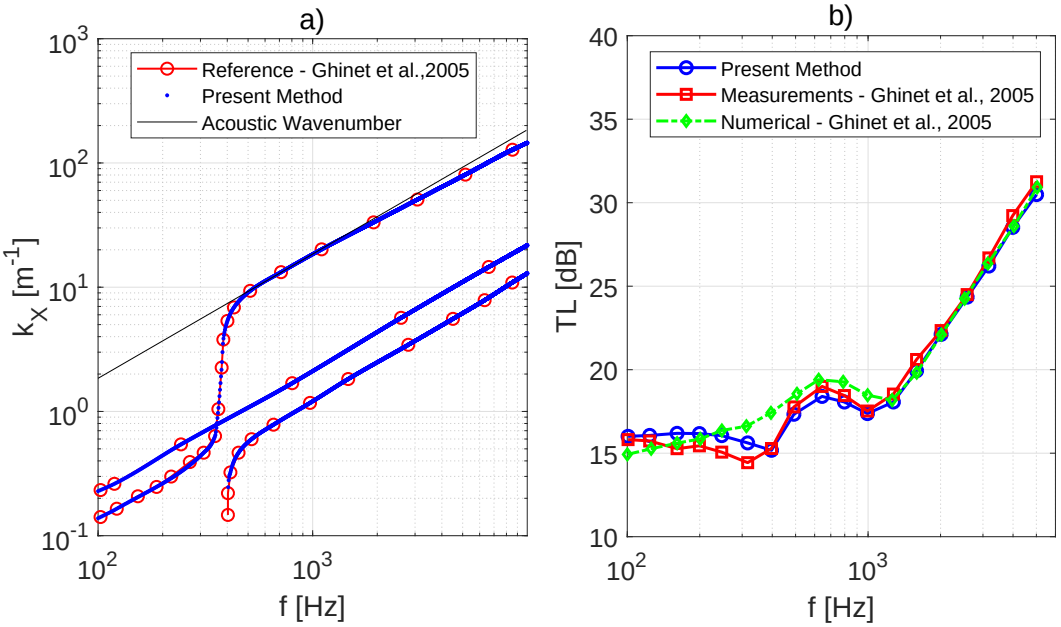

Figure 11: A finite curved sandwich composite panel under diffuse acoustic field excitation. a) Dispersion Curves comparison with results from [29]. b) TL comparison with measurements from [29] are compared with the actual method, in third octave bands.

Table 2: Geometrical parameters of the ribbed fuselage panel.

	Frames	Stringers	Skin
Thickness (mm)	1.8	1.2	1.2
Height (mm)	72	28	
Spacing (mm)	40.6	15.2	

4.4. Curved Complex Panel

In this subsection a final test-case is studied: a doubly-ribbed curved fuselage panel with fames and stringers. The structure is characterised by a strong heterogeneity and complexity and sound transmission loss measurements, from [24], are used as reference results. The panel has dimensions 1.45 m x 1.70 m, with a 1.35 m radius of curvature; the geometrical parameters are reported in Table 2, while the material is an aluminium alloy for all its substructures [24]. An illustration of the panel and the relative substructure used within this WFE-based framework, are shown in Fig. 12. It can be observed from Fig. 12, that the real panel has non periodic elements at the borders; some differences between the real structure and the ideally periodic model we assume within this approach, are thus present.

The modelled periodic cell has more than $2.9 \cdot 10^4$ degrees of freedom, that are reduced to $6.0 \cdot 10^4$ using the modal order reduction described in Section 2. Here, the finite size effects are accounted using the approximation in Eq. (24). In Fig. 13, a good agreement is observed in the 300 Hz - 2.0 kHz frequency range with the experimental measurements from [24, 25]. Both the numerical and experimental TL curves drop around the ring frequency ($\approx$ 630 Hz; [24, 25]). This

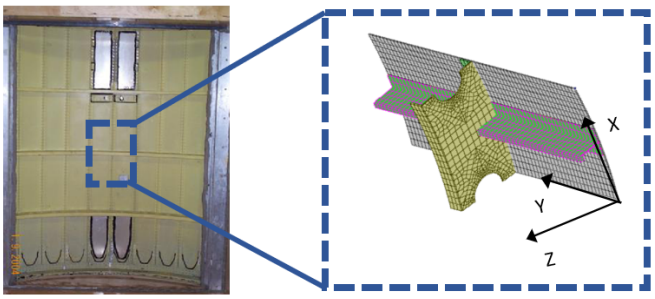

Figure 12: The panel tested in [25] and the unit cell used for the WFE simulation: cell sizes are coherent with the stiffeners spacing in Table 2.

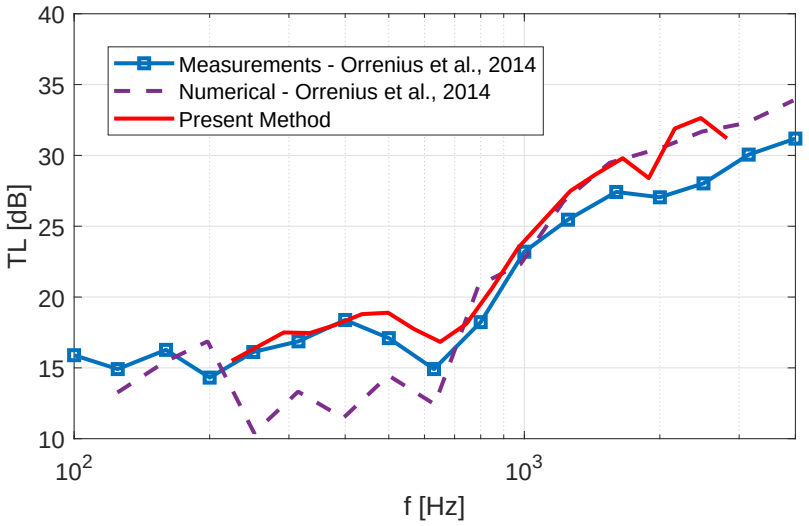

Figure 13: The Sound Transmission Loss of a curved ribbed panel under diffuse acoustic field; comparison with numerical and experimental results form [24].

inversely proves that, even for such a complex-shaped structure, the curvature simulation presented in Eq. (10) is still applicable (L_x/R still small enough).

5. Validation for Boundary Layer Transmission

The load approximation proposed in Section 3, leading to Eq. (22), allows the simulation for loads with different characteristics. In this section, for example, the flow-induced transmission caused by turbulent boundary layer (TBL) excitation is considered. This is known for being one of the main sources of radiated noise inside an aircraft cabin, in cruise flight conditions.

While many boundary layer models are proposed in literature, here, the characterisation of the wall pressure fluctuations proposed by Corcos is used [40, 39]. It is assumed that no-gradients effects are present and the TBL is fully developed. The wavenumber spectra, Φ_{PP}, proposed by Corcos, is here reported for the sake of completeness assuming the directions X and Y as the stream-wise and cross-wise ones:

$$\Phi_{PP}(k_X, k_Y, \omega) = S_{pp}(\omega) \frac{4\alpha_X \alpha_Y}{\left[\alpha_Y^2 + \frac{U_c^2 k_Y^2}{\omega^2}\right]\left[\alpha_X^2 + \left(1 + \frac{U_c k_X}{\omega}\right)^2\right]} \tag{25}$$

where U_c is the convective flow speed, S_{pp} is the single-point auto spectral density of the wall pressure distribution. The stream-wise and cross-wise correlation coefficients, α_X and α_Y, are assumed to be 0.125 and 0.78, respectively, in all following test-cases.

First, a validation for the boundary layer transmission, in the case of a flat isotropic panel with simply-supported boundary conditions (edges), is proposed in Fig. 14. The reference solution is calculated using a full FE method, as proposed, and validated, in many works in literature [1, 5]. The eigen-frequencies and the modal shapes of the reference panel are calculated using analytic solutions, while the load matrix is described using a direct method [1]. The incident power, for the transmission loss calculation, in the FEM cases, is calculated using Eq. (26) as proposed in literature [7, 41]:

$$\Pi_{\text{inc}} = \frac{A S_{pp}(\omega)}{4\rho_1 c_1} \tag{26}$$

where A is the excited area and c_1 the speed of sound on the incident side. A modal behaviour can not be described using the present method, as in an SEA framework, since the wave propagation is considered to the infinite (reflections at the borders are neglected) and a semi-infinite fluid termination is assumed (no internal cavity modes). The averaged sound transmission losses are calculated in discrete frequencies (in logarithmic space), while the FEM calculation is in third octaves bands. In both the test-cases proposed here, the dispersion curves in the flow direction (X) is provided in order to show the convective/aerodynamic and acoustic coincidences.

For the aluminium case (Fig. 14), the aerodynamic and acoustic coincidences are at $\approx$ 1.6 kHz and $\approx$ 6.0 kHz, as shown in the dispersion curves in Fig. 14a. Here, the finite size effects are accounted using a radiation efficiency formulation for flat panels, as proposed by Leppington [10]. As shown in Fig. 14b, both the aerodynamic and acoustic coincidence dips are correctly identified

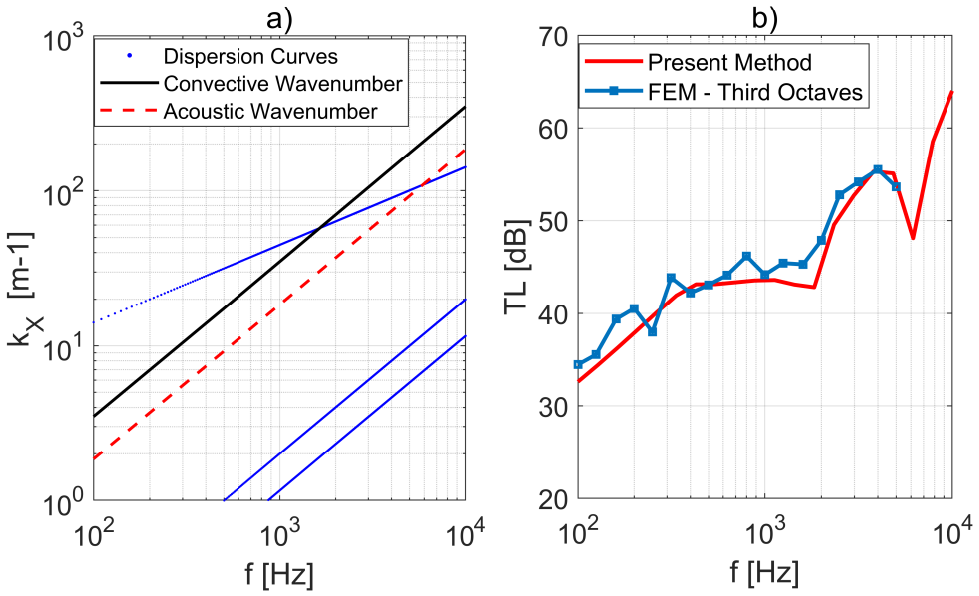

Figure 14: An aluminium plate under TBL excitation: a) Dispersion curves with convective and acoustic wavenumbers; b) TL numerical comparison with full FEM - $U_c = 180$ m/s; A = 0.5x0.3m^2. A logarithmic frequency step, between 100 Hz and 10KHz, is used to generate the curve labelled as *Present Method*.

in the sound transmission curves, as shown by the comparison with the octaves averaged FEM solution. The convective load induces a smoother and damped coincidence effect, with respect to the acoustic one.

Differently, an honeycomb–cored sandwich panel is analysed under a turbulent boundary layer in Fig. 15. A Corcos model is used for the loading description and the proposed approximation into surface waves is used. The panel is made of 1mm-thick aluminium skins and a 10mm-thick hexagonal Nomex honeycomb core (material properties in Table 1), homogenised in an equivalent orthotrophic model. Both the aerodynamic and acoustic coincidences are well predicted in the sound transmission loss curves, in Fig. 15b. The first one is somewhat highly damped ($\approx$ 600 Hz; see Fig. 15a) while the second one is clearly visible ($\approx$ 9 KHz; Fig. 15a).

The strong agreement observed in Fig. 14 and 15, validates the proposed load approximation even for spatially-correlated random loads, as the TBL. It is worth underlying how the use of boundary layer excitation is here allowed even for infinite structures, differently from other methods in literature [7].

5.1. The Effective Transmission Loss of Cylinders

In the case of shells, the load is translated in helical waves, instead of wall plane waves. For example, the effective transmission loss of a shell, in the case of simultaneous acoustic and aerodynamic excitation, can be estimated, assuming the axial direction of the shell as the stream-wise and the circumferential as an approximated cross-wise. In Fig. 16 the dispersion curves in the circumferential direction (wavenumbers of purely circumferential waves) are plotted for three different 3.2mm-thick aluminium shells; 3.0, 2.0 and 0.75 m curvature radii are considered and the

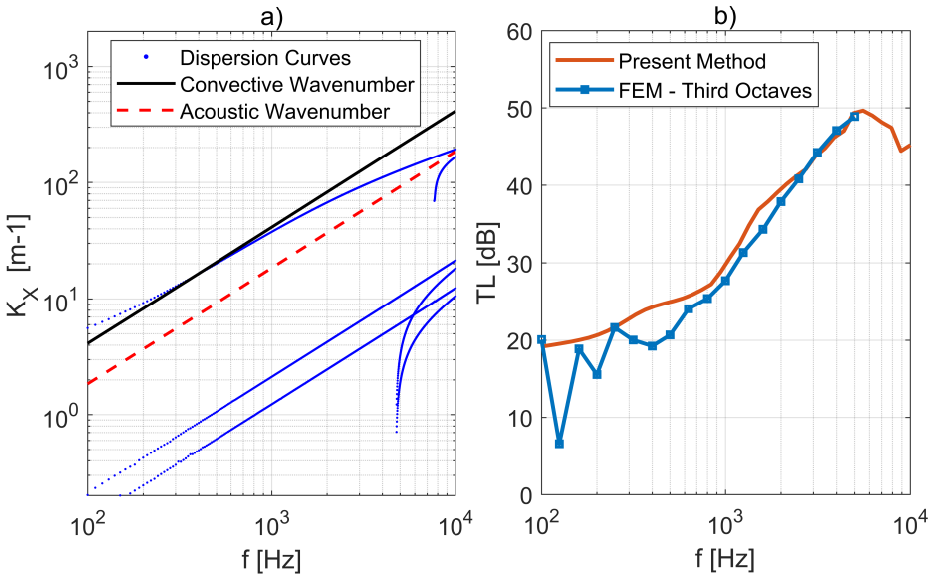

Figure 15: An honeycomb sandwich plate under TBL excitation: a) Dispersion curves with convective and acoustic wavenumbers; b) TL numerical comparison with FEM method - U_c = 152 m/s; A = 0.8x0.6m^2. A logarithmic frequency step, between 100 Hz and 10KHz, is used to generate the curve labelled as *Present Method*.

ring frequencies are, respectively, 280, 400 and 1090 Hz. Differently, in Fig. 17, the effective transmission loss is calculated and compared. The aim, in this case, is to investigate how the aerodynamic coincidence influences the shell transmission.

In the case of the two bigger cylinders (see Fig. 16), the ratio between the ring frequency and the aerodynamic coincidence frequency is lower than one (on the flat case the radius equal to infinite). Right after the ring frequency, when the curvature effects start to vanish, these shells still behave in a sub-convective domain, thus, the effects of the coincidence are clearly visible in the sound transmission loss (see Fig. 17). On the other hand, in the case of the small cylinder, the ring frequency is superior to the critical aerodynamic frequency and the shell behaves in a sub-convective domain only when the curvature effects are important. The aerodynamic coincidence peak, in the transmission loss, is no more identifiable.

Similarly, if a single shell is analysed under different convective speeds, the aerodynamic coincidence region moves in accordance to what happens in the operative conditions of a transport system as an aircraft, a train or a vehicle. The boundary layer effect vanishes when the speed lowers, since, the convective critical frequency lowers, up to getting inferior to the ring frequency.

6. Discussion on approximations and limits

It is useful to discuss and emphasize some aspects regarding the approximations and the limits of the present numerical method, presented in Sections 2 and 3, using as reference and illustrative schemes Figs. 1, 2, 3, 4 and 5.

The curvature simulation in Eq. (10), is a good approximation for homogenised models. For periodic non-homogenised models, relatively small curvatures can be simulated. In fact, when the

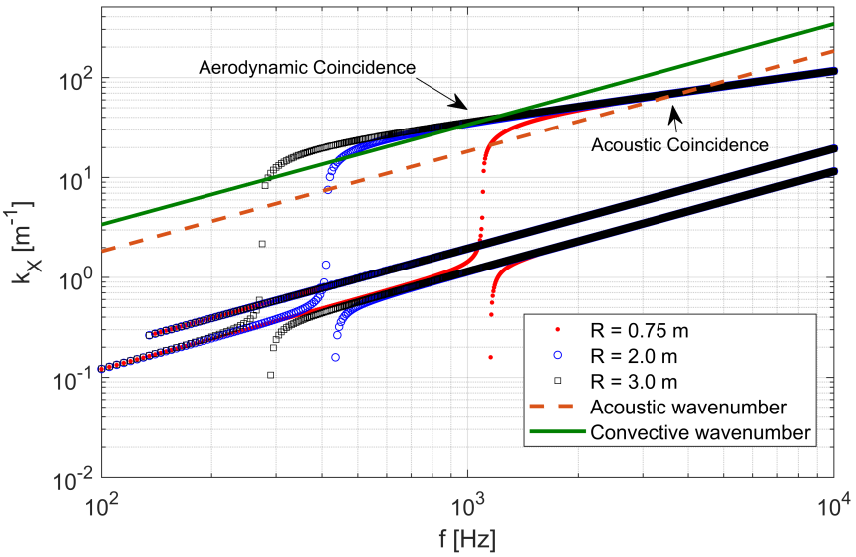

Figure 16: Dispersion curves in the circumferential direction of shells of different curvature. The acoustic and convective ($U_c = 185$ m/s) wavenumbers are shown.

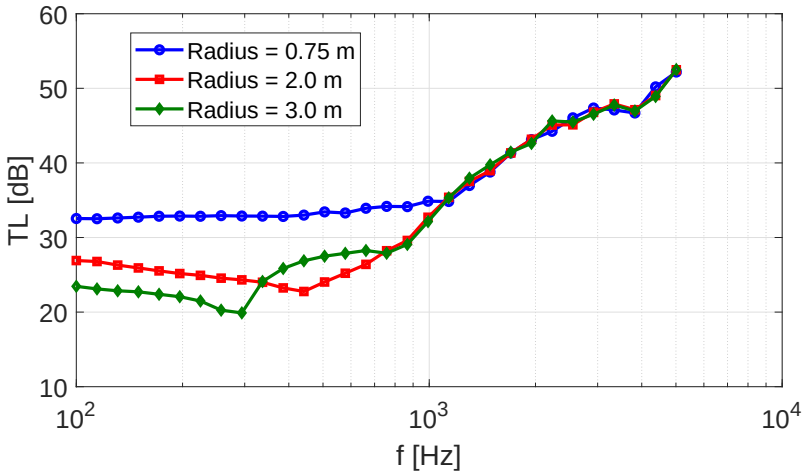

Figure 17: The effective transmission loss for shells of different curvature - $U_c = 185$ m/s. A logarithmic frequency step, between 100 Hz and 5KHz, is used to generate the curves.

ratio between the length of the cell (in the curvature direction) and the radius of curvature is not small enough, the piecewise-flat approximation used here is critical even for fine structural meshes. In addition, great care must be placed on not curving even potential internal elements which can be flat (i.e resonator beams).

The interior acoustic field, as illustrated in Fig. 4, is assumed to be equivalent to a semi-infinite fluid termination: the modal behaviour of a finite cavity can not be described in this context, even for a closed cylindrical model. In analogy to what happens for an infinite flat structure, the internal acoustics is assumed to be composed by single out-going waves and internal acoustic waves' reflections/transmission are not modelled (see Eq. (13)). These are the same assumptions/approximations used in [29, 30].

The method provides good results, as expected, in the limit where the periodic length is small compared to structural and acoustic wavelengths: homogenised (or smeared) models are enough for a correct description of the wave-guide. Nevertheless, the present comparisons, especially in Fig. 13, show a more general applicability well beyond the homogenisation limits and for large periodic scales. In fact, in this framework, the multiple harmonics that arise in the radiated acoustic field, for purely periodic (non-homogenised) structures, are numerically included in the structural response of the radiating side, when applying discrete periodic conditions for each couple of forcing wavenumbers k_X and k_Y. It, coherently to what has been discussed for the semi-infinite fluid termination condition, does not need to be analytically exploited since the only useful factor, in this method, for the acoustics in the radiating side is the k_Z term, dependent on the nature of the fluid itself (see Eq. (13)). In fact, when comparing the present approach with the work by Ghinet et al. [30], for an infinite isotropic cylinder under a diffuse acoustic field the agreement is excellent in the whole frequency band; the reference method, in [30], which is semi-analytical, properly describes the acoustic field in global coordinates, with a full development using spherical harmonics.

Moreover, the structural wave propagating in the periodic media is here considered to the infinite. In other words, waves' reflections, transmission and absorption, typical at the borders of a finite media, are not accounted and, thus, a single-modal behaviour can not be described with this model. However, the finite size effects, which help in re-scaling the sound transmission loss versus frequency (with respect to the one of an infinite structure) can be included in the model using correction factors, as described in [11].

Regarding the load approximation, the use of a lumped-on-the-nodes method, causes aliasing when the nodal areas are not small-enough to assume negligible pressure fluctuations within [1, 4]. While this approach is used because of its flexibility (the shape functions of the models are not required), it requires some care for convergence aspects. There are two main steps to check for a proper convergence. First, at cell scale, the single elements should have proper dimension to be able to describe the smallest wavelengths at the maximum frequency of analysis. This is a well-known mesh sizing problem. In the present work, more than 6 (in some cases more than 10) elements per minimum wavelength have been used. Here, the approximation described in Section

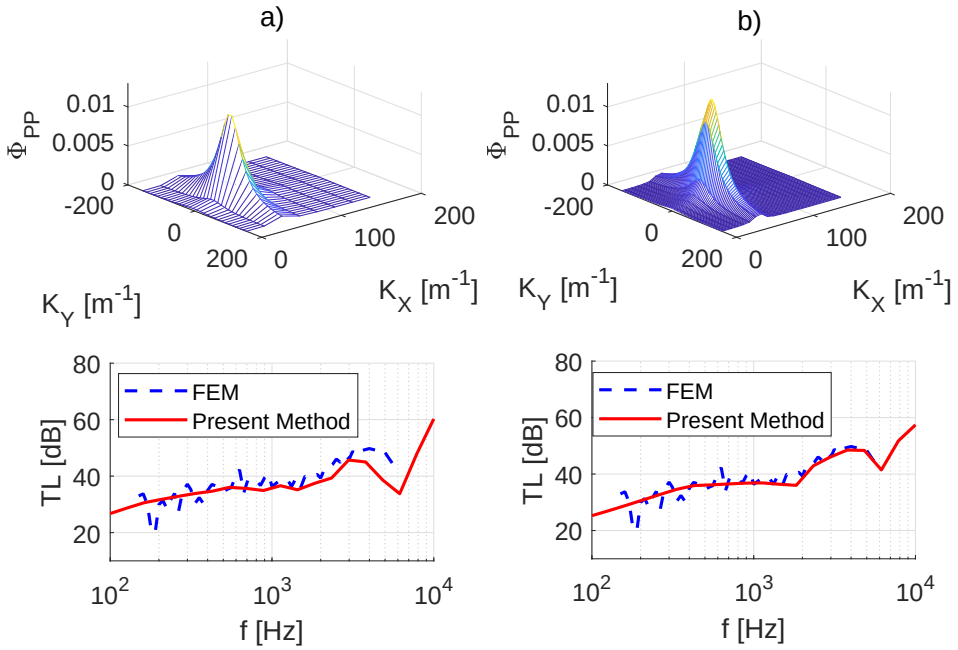

Figure 18: The transmission loss of an aluminium panel under TBL excitation; numerical comparison with full FEM method in octaves - U_c = 180 m/s; A = 0.7x0.5m^2. a) Coarse meshing of the TBL wavenumber spectra; b) Fine meshing of the TBL wavenumber spectra

3, releases the constraints to the fluid/convective wavelength and allows a mesh design based on the pure structural dispersion curves.

Once the structural mesh sizing is performed, the integration scheme in Eq. (22) must be properly carried out. Depending on the wavenumber spectra of the excitation function, a proper mesh in the wavenumber space has to be used to describe the function $\Phi_{PP}(k_X, k_Y)$, at each frequency step. This is a typical discretization problem for functions of two variables. However, while an indiscriminate increase of the wavenumber sampling results in a more accurate integration, a strong increase of the number of operations can lead to high computational cost. A trade-off solution resulting from a convergence study, is strongly suggested. In Fig. 18, an example concerning the wavenumber integration is shown. In Fig. 18a a coarser mesh (wavenumber sampling with a 50x50 mesh) is used and, as a result, the TL predictions are not as accurate as expected. In Fig. 18b, on the contrary, a finer integration (wavenumber sampling with a 150x150 mesh) is applied and the results are very accurate broadband. This time, the reference solution is the same proposed in Fig. 14, in twelve octave bands.

A general rule is hard to define since the wavenumber spectra might differ widely, depending on the nature of the excitation. General numerical rules for the discretization of two-dimensional functions must be used case-by-case and a pre-calculation convergence study is suggested.

7. Conclusions

This work proposes a numerical approach for the estimation of the sound transmission loss of complex flat, curved and cylindrical periodic structures, under any type of acoustic and aerodynamic load. The approach involves a wave finite element method, for the structural part, and proposes a load simulation into surface waves. The fluid-structure interaction is performed in analogy to the acoustic wave excitation, discriminating among the different forcing models, using a weighted wavenumber integration. The only requirement is the knowledge of the wavenumber spectra of the wall pressure fluctuation. Finite size effects are accounted using the baffled window equivalence or asymptotic formulations, for flat structures. An alternative and efficient method is proposed in the case of curved finite structures, in similitude to the semi-infinite equivalent cases. Static and dynamic condensation can be applied if fine meshes are used in the modelling phase.

Both the accuracy and robustness of the present method are proved using analytic, numerical and experimental references. Both uncorrelated (diffuse acoustic field) and spatially-correlated loads (turbulent boundary layer) are used for the validations, in the case of flat and curved structures. Calculations performed using finite elements of different nature do not affect the accuracy of the estimations. The convergence of the approach is assured by the one of the wavenumber integration process. The choice of the integration limits must be calculated on the base of the wavenumber spectra of the load.

The combination of boundary layer and acoustic excitation is simulated in the case of shells, resulting in an effective sound transmission loss. The ring frequency, the aerodynamic and acoustic coincidences are efficiently estimated, independently on the curvature radius and convective velocity simulated. Moreover, the use of boundary layer excitation does not require the accounting of finite size effects and a comparison of the structural and acoustic design is possible, independently from the size of the analysed structure.

Acknowledgments

This project has received funding from the European Unions Horizon 2020 research and innovation programme under the Marie Sklodowska-Curie grant agreement No. 675441. The author would like to gratefully acknowledge everyone involved in the VIPER project.

References

[1] F. Franco, S. De Rosa, E. Ciappi, Numerical approximations on the predictive responses of plates under stochastic and convective loads, J. Fluid Struct. 42 (2013) 296–312. doi:/10.1016/j.jfluidstructs.2013.06.006.

[2] M. Ichchou, B. Hiverniau, B. Troclet, Equivalent rain on the roof loads for random spatially correlated excitations in the mid frequency range, J. Sound Vib. 322 (2009) 926–940. doi:/10.1016/j.jsv.2008.11.050.

[3] S. Hambric, Y. Hwang, W. Bonness, Vibrations of plates with clamped and free edges excited by low-speed turbulent boundary layer flow, J. Fluid Struct. 19 (1) (2004) 93–110. doi:/10.1016/j.jfluidstructs.2003.09.002.

[4] S. De Rosa, F. Franco, A scaling procedure for the response of an isolated system with high modal overlap factor, Mech. Syst. Signal Process. 22 (2008) 1549–1565. doi:/10.1016/j.ymssp.2008.01.007.

[5] S. De Rosa, F. Franco, Exact and numerical responses of a plate under a turbulent boundary layer excitation, J. Fluid Struct. 24 (2008) 212–230. doi:/10.1016/j.jfluidstructs.2007.07.007.

[6] J. Allard, N. Atalla, Propagation of sound in porous media: Modelling sound absorbing materials, John Wiley & Sonsdoi:/10.1002/9780470747339.

[7] N. Atalla, Modelling the sound transmission through complex structures with attached noise control materials, Wave Motion 51 (2014) 650–663. doi:/10.1016/j.wavemoti.2013.11.001.

[8] A. Parrinello, G. Ghiringhelli, Transfer matrix representation for periodic planar media, J. Sound Vib. 371 (2016) 196–209. doi:/10.1016/j.jsv.2016.02.005.

[9] D. Rhazi, N. Atalla, A simple method to account for finite size effects in the transfer matrix method, J. Acoust. Soc. Am. 127 (2) (2010) EL30–EL36. doi:/10.1121/1.3280237.

[10] F. Leppington, E. Broadbent, K. Heron, The acoustic radiation efficiency from rectangular plates, Proc. R. Soc. 382 (1982) 245–271. doi:/10.1098/rspa.1982.0100.

[11] M. Villot, C. Guigou, L. Gagliardini, Predicting the acoustical radiation of finite size multi-layered structures by applying spatial windowing on infinite structures, J. Sound Vib. 245 (3) (2001) 433–455. doi:/10.1006/jsvi.2001.3592.

[12] L. Brillouin, Wave propagation in periodic structures: Electric filters and crystal lattices, 2nd edition Dover Publications (Mineola, New York). doi:10.1016/S0031-8914(53)80099-6.

[13] D. Mead, Wave propagation in continuous periodic structures: research contributions from southampton, J. Sound Vib. 190 (3) (1996) 495–524. doi:/10.1006/jsvi.1996.0076.

[14] E. Manconi, B. R. Mace, Modelling wave propagation in two dimensional structures using finite element analysis, J. Sound Vib. 318(45) (2008) 884–902. doi:/10.1016/j.jsv.2008.04.039.

[15] F. Errico, M. Ichchou, S. De Rosa, O. Bareille, F. Franco, The modelling of the flow-induced vibrations of periodic flat and axial-symmetric structures with a wave-based method, J. Sound Vib. 424 (2018) 32–47. doi:/10.1016/j.jsv.2018.03.012.

[16] J. M. Renno, B. R. Mace, Calculating the forced response of cylinders and cylindrical shells using the wave and finite element method, J. Sound Vib. 333 (21) (2014) 5340–5355. doi:/10.1016/j.jsv.2014.04.042.

[17] J. M. Renno, B. R. Mace, Vibration modelling of structural networks using a hybrid finite element/wave and finite element approach, Wave Motion 51 (4) (2014) 566–580. doi:/10.1016/j.wavemoti.2013.09.001.

[18] J. Morsbol, S. Sorokin, Elastic wave propagation in curved flexible pipes, Int. J. Solid Struct.75–76 (2015) 143–155. doi:/10.1016/j.ijsolstr.2015.08.009.

[19] E. Manconi, B. R. Mace, Wave characterization of cylindrical and curved panels using a finite element method, J. Acoust. Soc. Am. 125 (1) (2009) 154–163. doi:/10.1121/1.3021418.

[20] E. Manconi, B. R. Mace, R. Garziera, The loss-factor of pre-stressed laminated curved panels and cylinders using a wave and finite element method, J. Sound Vib. 332 (7) (2013) 1704 – 1711. doi:/10.1016/j.jsv.2012.09.039.

[21] E. Manconi, B. R. Mace, Estimation of the loss factor of viscoelastic laminated panels from finite element analysis, J. Sound Vib. 329 (19) (2010) 3928 – 3939. doi:/10.1016/j.jsv.2010.04.014.

[22] J.-L. Christen, M. Ichchou, A. Zine, B. Troclet, Wave finite element formulation of the acoustic transmission through complex infinite plates, Acta Acustica united with Acustica 102(6) (2016) 984–991. doi:/10.3813/AAA.919013.

[23] Y. Yang, B. Mace, M. Kingan, Prediction of sound transmission through, and radiation from, panels using a wave and finite element method, J. Acoust. Soc. Am. 141 (4) (2017) 2452–2460. doi:/10.1121/1.4977925.

[24] U. Orrenius, H. Liu, A. Wareing, S. Finnveden, V. Cotoni, Wave modelling in predictive vibro-acoustics: Applications to rail vehicles and aircraft, Wave Motion 51 (4) (2014) 635–649. doi:/10.1016/j.wavemoti.2013.11.007.

[25] U. Orrenius, V. Cotoni, A. Wareing, Analysis of sound transmission through aircraft fuselages excited by turbulent boundary layer or diffuse acoustic pressure fields, 38th International Congress and Exposition on Noise Control Engineering 2009, INTER-NOISE 2009 4 (2009) 2637–2645.

[26] L. Koval, On sound transmission into an orthotropic shell, J. Sound Vib. 63 (1) (1979) 51–59. doi:/10.1016/0022-460X(79)90376-6.

[27] L. Koval, Sound transmission into a laminated composite cylindrical shell, J. Sound Vib. 71 (4) (1980) 523–530. doi:/10.1016/0022-460X(80)90724-5.

[28] L. Koval, On sound transmission into a thin cylindrical shell under flight conditions, J. Sound Vib. 48 (2) (1976) 265–275. doi:/10.1016/0022-460X(76)90465-X.

[29] S. Ghinet, N. Atalla, H. Osman, The transmission loss of curved laminates and sandwich composite panels, J. Acoust. Soc. Am. 118 (2) (2005) 774–790. doi:/10.1121/1.1932212.

[30] S. Ghinet, N. Atalla, H. Osman, Diffuse field transmission into infinite sandwich composite and laminate composite cylinders, J. Sound Vib. 289 (2006) 745–778. doi:/10.1016/j.jsv.2005.02.028.

[31] B. Liu, L. Feng, A. Nilsson, Sound transmission through curved aircraft panels with stringer and ring frame attachments, J. Sound Vib. 300 (2007) 949–973. doi:/10.1016/j.jsv.2006.09.008.

[32] B. Liu, Noise radiation of aircraft panels subjected to boundary layer pressure fluctuations, J. Sound Vib. 314 (2008) 693–711. doi:/10.1016/j.jsv.2008.01.045.

[33] M. Kingan, Y. Yang, B. Mace, Application of the wave and finite element method to calculate sound transmission through cylindrical structures, J. of Phys.: Conf.Series 744 (1) 012240. URL http://stacks.iop.org/1742-6596/744/i=1/a=012240

[34] C. Droz, C. Zhou, M. Ichchou, J.-P. Laine, A hybrid wave-mode formulation for the vibro-acoustic analysis of 2d periodic structures, J. Sound Vib. 363 (2016) 285–302. doi:/10.1016/j.jsv.2015.11.003.

[35] C. Droz, J.-P. Laine, M. Ichchou, G. Inquiete, A reduced formulation for the free-wave propagation analysis in composite structures, Compos. Struct. 113 (2014) 134–144. doi:/10.1016/j.compstruct.2014.03.017.

[36] C. Zhou, J.-P. Laine, M. Ichchou, A. Zine, Wave finite element method based on reduced model for one-dimensional periodic structures, Int. J. App. Mech. 7 (2) (2015) 32–47. doi:/10.1142/S1758825115500180.

[37] D. Chronopoulos, B. Troclet, M. Ichchou, J.-P. Laine, A unified approach for the broadband vibroacoustic response of composite shells, Comp. Part B: Eng. 43 (2013) 1837–1846. doi:/10.1016/j.compositesb.2012.01.059.

[38] B. Mace, Sound radiation from fluid loaded orthogonally stiffened plates, J. Sound Vib. 79 (3) (1981) 439–452. doi:https://doi.org/10.1016/0022-460X(81)90321-7.

[39] W. Graham, A comparison of models for the wavenumber-frequency spectrum of turbolent boundary layer pressures, J. Sound Vib. 206(4) (1997) 541–565. doi:/10.1006/jsvi.1997.1114.

[40] G. Corcos, Resolution of pressure in turbulence, J. Acoust. Soc. Am. 35 (1963) 192–199. doi:/10.1121/1.1918431.

[41] L. Barisciano Jr, Broadband transmission loss due to reverberant excitation, NASA/CR-1999-209687, Langley Research Center, Hampton, Virginia.